Received: 28 April 2017 | Revised: 16 July 2017 | Accepted: 9 September 2017

DOI: 10.1002/gj.3047

WILEY

SPECIAL ISSUE ARTICLE

Late Miocene magnetostratigraphy of Jianzha Basin in the northeastern margin of the Tibetan Plateau and changes in the East Asian summer monsoon

Chaofeng Fu[1,2] | Xiaoke Qiang[2] | Xinwen Xu[3] | Jianjian Xi[1] | Jun Zuo[1] | Zhisheng An[2]

[1]The School of Earth Science and Resources, Chang'an University, Xi'an, Shaanxi, China

[2]State Key Laboratory of Loess and Quaternary Geology, Institute of Earth and Environment, CAS, Xi'an, Shaanxi, China

[3]College of Urban and Environmental Science, Northwest University, Xi'an, Shaanxi, China

Correspondence
C. Fu, The School of Earth Science and Resources, Chang'an University, Xi'an, 710054, China.
Email: fucf@chd.edu.cn

Funding information
National Natural Science Foundation of China, Grant/Award Number: 41772167, 41572164, 41140028, 40872114 and 40599420; State Key Laboratory of Loess and Quaternary Geology, Grant/Award Number: SKLLQG1601; Central University Research Foundation, Chang'an University, Grant/Award Number: 310827152014

Handling Editor: S. Li

Jianzha Basin is located in the northeastern Tibetan Plateau (NETP) and contains a thick sequence of Cenozoic sediments that are an archive of information about the growth of the Tibetan Plateau and the evolution of the arid environment of the interior of Asia. Here, we present magnetostratigraphic and palaeoenvironmental records from a 361-m-thick sequence of Late Cenozoic eolian Red Clay and intercalated fluviolacustrine deposits in the Jianzha Basin. The magnetostratigraphic results show that the sediments have recorded a continuous geomagnetic polarity sequence from C5r.3r to C3r, spanning the interval from 11.8 to 5.8 Ma in the Late Miocene. There are two intervals of rapidly fluctuating sedimentation rates between ~10 and ~6 Ma, which we interpret as a response to a series of uplifts and expansions to the north and to the east in the NETP. The fluctuations in Rb/Sr ratio and magnetic susceptibility before ~8.57 Ma reflect intensified East Asian summer monsoon (EASM) precipitation which resulted from the growth of the NETP. From ~8.57 to ~7.21 Ma, the EASM was impacted by global cooling and ice build-up in the Northern Hemisphere in addition to the uplift of the Tibetan Plateau (TP) in the Late Miocene. From ~8.57 to ~7.21 Ma, there is a lack of coherency between the fluctuations in MS and Rb/Sr ratio; however, subsequently, there is significant coherency between the Rb/Sr ratio and the deep-sea oxygen isotope record present. This suggests that from ~8.57 Ma, the eolian Red Clay sediments in the Jianzha Basin were significantly affected by the addition of dust derived from the deforming and uplifting areas of the TP.

KEYWORDS

East Asian summer monsoon, Jianzha Basin, Late Miocene, magnetostratigraphy, Northeast Tibet Plateau

1 | INTRODUCTION

The growth of the Tibetan Plateau (TP) and the surrounding mountains have had a major impact on the initiation and evolution of the Asian monsoon climate on tectonic timescales (An, Kutzbach, Prell, & Porter, 2001; Clift, Wan, & Blusztajn, 2014; Kutzbach, Guetter, Ruddiman, & Prell, 1989; Liu et al., 2015; Prell & Kutzbach, 1992; Yin, 2010; Zhang, Wang, Guo, & Jiang, 2007). A significant effort has been made to understand the impact of the uplift of the TP and global cooling on climate change in Asia, and the findings have significantly improved our understanding of when and how the Asian monsoon developed (An et al., 2001; Fu, Bloemendal, Qiang, Hill, & An, 2015; Guo et al., 2002; Kutzbach et al., 1989; Liu et al., 2015; Molnar, England, & Martinod, 1993; Prell & Kutzbach, 1992; Raymo & Ruddiman, 1992; Rea, Snoeckx, & Joseph, 1998; Sun et al., 2015). Based on variations of climate proxies from Chinese eolian deposits and sediment cores from the South China Sea, the initiation of the Asian monsoon has been extended back to at least the late Oligocene–early Miocene transition (An et al., 2006; Clift et al., 2014; Guo et al., 2002; Lu & Guo, 2014; Qiang et al., 2011; Shi, Tang, & Ma, 1999; Sun & Wang, 2005).

The climate of the northeastern Tibetan Plateau (NETP) is influenced by several atmospheric circulation systems: the mid-latitude Westerlies, the Asian winter monsoon, the Asian summer monsoon (ASM), and the ASM system, comprising two subsystems of the East Asian summer monsoon (EASM) and the Indian monsoon (IM; Figure 1a). A recent study concluded that since the Eocene, IM

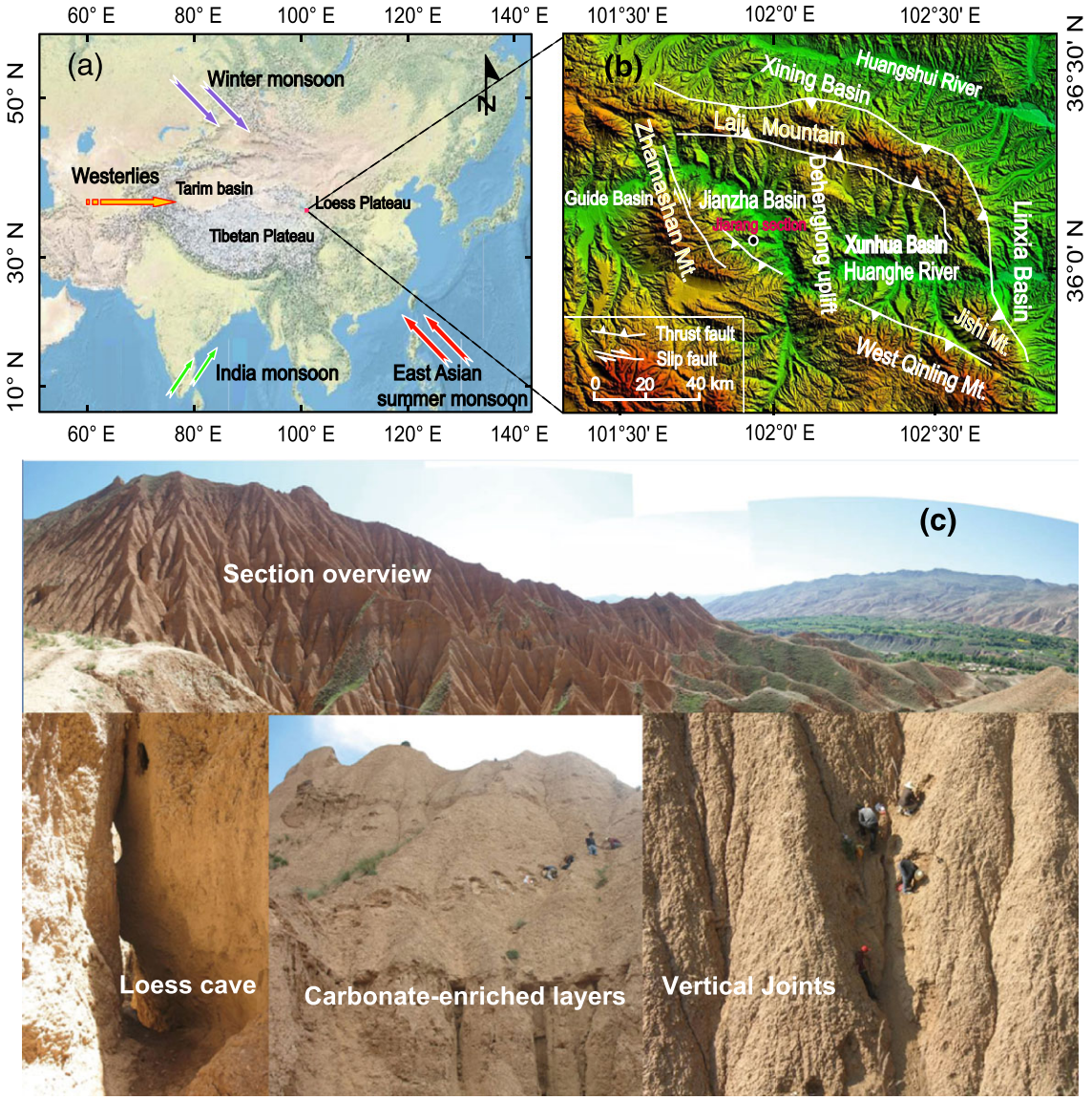

FIGURE 1 (a) Location of the study section in the Jianzha Basin, major geographic features, and atmospheric circulation systems. (b) Major structural and geomorphological features of the area surrounding Jianzha Basin. (c) View of the study section, showing microtopography and stratigraphic characteristics

moisture has been unable to reach the central TP because of the southern topographic barrier (Caves et al., 2015). The link between monsoon strength and elevation of the TP is intriguing, but has not been convincingly demonstrated, not least because of the lack of detailed knowledge about the growth of the plateau and the sparsity of long-term records of monsoon evolution (Wan, Clift, Li, Li, & Yin, 2010). Records of dust accumulation in the North Pacific Ocean and the onset of loess accumulation in the central Chinese Loess Plateau (CLP) at ~8 Ma (An et al., 2001; Qiang, Li, Powell, & Zheng, 2001; Rea et al., 1998) are regarded as indicators of the aridification of the Asian interior from the Late Miocene. However, this inference is in contradiction with evidence for a strengthening of the EASM precipitation driven by the growth of the TP at ~8 Ma (Nie et al., 2017). Thus, reconstructing late Miocene changes in the EASM from the sedimentary sequences in the Asian interior and the NETP is important for increasing our understanding of the late Cenozoic climatic evolution of Asia.

The Qaidam–Qilian active block is a part of the NETP, which is the leading edge of the terrane generated by the expansion of the plateau towards mainland Eurasia. The area plays an important role in continental dynamics and in the large-scale interaction between the lithosphere and the atmosphere (Fang et al., 2005; Métivier, Gaudemer, Tapponnier, & Meyer, 1998; Molnar & Lyon-Caent, 1989; Tapponnier et al., 1990). Previous palaeoclimatic records come mainly from the CLP on the periphery of the TP (An, 2000; An et al., 2001; Ding et al., 1998; Ding, Rutter, Sun, Yang, & Liu, 2000; Qiang et al., 2001; Qiang et al., 2011; Sun et al., 2006; Sun, An, Clemens, Bloemendal, & Vandenberghe, 2010; Sun, Shaw, An, Cheng, & Yue, 1998), and some lacustrine sedimentary sequences from the NETP (An et al., 2012; Fu et al., 2013; Song et al., 2014). However, eolian records from the interior of the TP are rare. The Jianzha Basin is located in the NETP and contains a thick sequence of Cenozoic sediments which provide a record of the evolution of the arid environment of the Asian interior. In this study, we present the results of palaeomagnetic and

geochemical analyses of the eolian Red Clay sequence and intercalated fluviolacustrine deposits from the Jianzha Basin. Our aims are (1) to establish a high-resolution magnetostratigraphy for the continuous and well-exposed sedimentary sequence in the Miocene in the Jianzha Basin to provide a chronology for ongoing palaeoenvironmental studies of the region; (2) to reconstruct the history of chemical weathering of the NETP, related to EASM precipitation, for the Late Miocene based on magnetic susceptibility (MS) and geochemical measurements; and (3) to elucidate possible links between the EASM and the uplift of the TP, as well as other controls on EASM evolution such as changes in global ice volume.

2 | GEOLOGICAL SETTING, LITHOLOGY, AND SAMPLING

The Jianzha Basin experienced a series of uplift events during the Miocene: of the eastern LaJi Shan by ca. 22 Ma, the Zamazari Shan by ca. 20 Ma, the JiShi Shan by ca. 13 Ma, and the growth of the western LaJi Shan and Riyue Shan at 8–10 Ma, and subsequently, the basin was separated by a series of mountains or uplands controlled by a WNW- and NNW-striking thrust fault to the west of the Guide Basin, to the north of the Xining Basin and to the east of the Xunhua Basin and the Linxia Basin (Hough, Garzione, Wang, & Lease, 2014; Figure 1b). The Jianzha Basin is situated in a climatically sensitive area—at the transition zone between the monsoon region to the east and the arid region to the west; the current annual rainfall varies from 200 to 400 mm (An et al., 2006; Li, 1991; Li & Fang, 1999; Li, Feng, & Tang, 1988; Figure 1a); its location, together with its thick, continuous sequence of Cenozoic sediments, makes it well suited to monitoring changes in Late Cenozoic climate.

Previous studies have established a basin-wide lithostratigraphic framework for the Guide–Hualong Basin. The Cenozoic stratigraphy, from the Oligocene to the Pliocene, throughout the peripheral basin has been divided into the Xining Group (including the Nengguo Formation and Andang Formation) and the Guide Group (including the Garang, Xiadongshan, Herjia, and Ganjia formations) (Song, Fang, Gao, Sun, & Fan, 2001). However, Gu et al. (1992) divided the Guide Group into the Chetougou, Xianshuihe, Charang, Xiadongshan, and Shangtan formations. From a comparison with the lithology and strata of the peripheral basin, the exposed section investigated in the Jianzha Basin can be divided into the Late Miocene Xiadongshan and Jiarang formations in this text (Figure 2). Field investigations of a section (35°57′43.1″N, 101°58′24.1″E) near Jiarang Village indicated that the strata are approximately horizontal, continuous, and well exposed, with a thickness of about 360 m (Figure 1c). Based on field observations, the sediments of the Jiarang Village section mainly consist of clastic material of fluviolacustrine and eolian origin, with loess-like silt or clay comprising about two-thirds of the entire section (Figure 2). The lower part (361–22.8 m) can be divided into three lithological subunits: (i) 361–271.4 m. Yellow-brown earth sediments (Red Clay), with pale, leached carbonate-enriched layers, similar to the horizons of re-precipitated carbonate in Quaternary loess deposits (Guo et al., 1998). Vertical joints are well developed in the section, and gullies have formed along the vertical joints (Figure 1c; Sun, 2005). The sedimentological characteristics of the yellow-brown silts in the Jianzha Basin are very similar to those of the Red Clay from the Loess Plateau, which are well-documented as being of eolian origin (Ding et al., 1998;

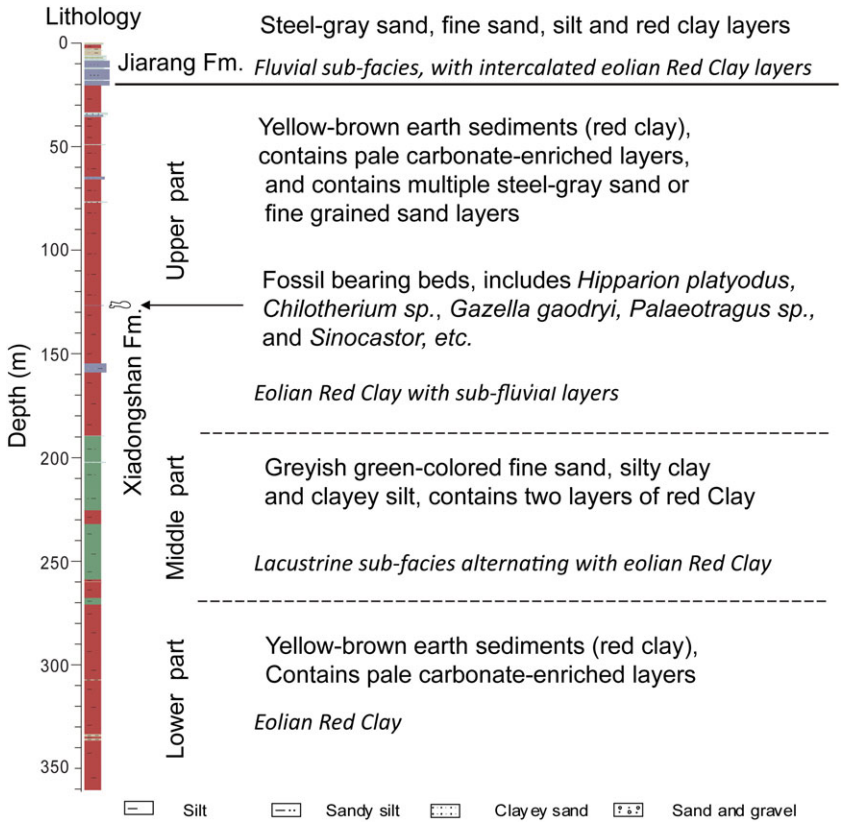

FIGURE 2 Lithology and sedimentary facies of the Jiarang section in Jianzha Basin. Location and composition of fossil mammal assemblages found within the section, and which provide a rough age constraint, are plotted on the left side of the stratigraphic column

Qiang et al., 2011). Therefore, we regard the lithology of this interval as eolian Red Clay. (ii) 271.4–187.2 m. Greyish green-coloured fine sand, silt clay, and clayey silt, containing two Red Clay layers. We interpret this interval as a lacustrine subfacies alternating with eolian Red Clay. (iii) 187.2–22.8 m. Red Clay, containing multiple steel-grey sand or fine sand layers, with several fossil-bearing carbonate beds at the depth of 128 m. We regard this as eolian Red Clay with subfluvial layers. The upper part of the section (22.8–0 m) consists of steel-grey fine gravel, coarse sand, fine sand, and silt, with occasional Red Clay layers. We interpret this interval as mainly a fluvial subfacies with intercalated eolian Red Clay layers.

About 1,800 powder samples were collected from the Jiarang Village section at an interval of 20 cm for rock magnetic and geochemical measurements. In addition, 1,729 oriented block samples, with dimensions of roughly $10 \times 10 \times 8$ cm^3, were taken at an interval of 20 cm for palaeomagnetic measurements. No samples were obtained from the coarse gravel layers in the section which comprised a total thickness of ~15 m.

3 | METHODS

3.1 | Magnetic measurements

The MS of low temperature oven-dried samples was measured at low (470 Hz) and high (4700 Hz) frequencies (χ_{lf} and χ_{hf}, respectively) using a Bartington Instruments meter and MS2B sensor. The frequency-dependent MS was calculated on a mass specific basis ($\chi_{fd} = \chi_{lf} - \chi_{hf}$) and as a percentage ($\chi_{fd}\% = 100 \times \chi_{hf}/\chi_{lf}$). The oriented block samples were cut into 2-cm cubes and used for thermal demagnetization of the natural remanent magnetization (NRM) using an ASC TD48 thermal demagnetizer and measured on a 2G Enterprises cryogenic superconducting magnetometer (Model 755R), installed in a magnetically shielded space (<300 nT). The samples were heated to 690 °C at temperature increments of 10–50 °C (see Figure 3). The demagnetization results were evaluated using orthogonal diagrams (Zijderveld, 1967), and the principal components directions were computed using a least-squares fitting technique (Kirschvink, 1980). All measurements were made at the Institute of Earth Environment, Chinese Academy of Sciences, Xi'an, China.

3.2 | The X-ray fluorescence (XRF) analyses

The concentrations of Rb and Sr were measured using an Olympus Delta Energy-Dispersive XRF (ED-XRF) analyser fitted with a robotic arm. The X-ray source was a 4 W rhodium x-ray tube (8–40 keV; 5–200 μA excitement) coupled with a thermo-electrically cooled large-area silicon drift detector. The detector window was covered with a thin (6 μm) polypropylene film to avoid contamination of the internal measurement sensors. The Olympus Delta in "Soil" mode applies three successive x-ray intensities (15, 40, and 40 [filtered] keV beam condition) and for "Mining plus" two successive x-ray intensities (15 and 40 keV beam condition). All measurements were made at the School of Environmental Sciences, University of Liverpool, UK.

4 | RESULTS

4.1 | Magnetostratigraphy

The intensity of NRM of the Red Clay and silt samples ranges from 1.5×10^{-4} to 7.2×10^{-5} A/m. Representative thermal demagnetization diagrams are shown in Figure 3. Most samples exhibit simple demagnetization behaviour. Below 50–200 °C, a viscous remanent magnetization (VRM) is removed (Figure 3). Between 100 and 150 °C and between 150 and 200 °C, many samples exhibit a significant decrease in magnetization accompanied by a change in the remanence direction that indicates the removal of a secondary remanent magnetization (SRM) carried by goethite and titanomagnetite, respectively (Figure 3a,c,d–f). In addition, most of the samples exhibit a low unblocking temperature component that is removed at 250 °C (Figure 3). Above this temperature, a characteristic remanent magnetization (ChRM) is clearly isolated and decays almost linearly to the origin. Three distinct and rapid reductions in magnetization were observed in most samples, at about 200 °C, 580 °C, 640 °C, and 660–690 °C, indicating the presence of titanomagnetite, magnetite, maghemite, and haematite, respectively (Liu et al., 2010; Thompson & Oldfield, 1986), and which are the major ChRM carriers (Figure 3).

Most of the samples yielded a stable ChRM component after stepwise thermal demagnetization up to 585 °C, which indicates that magnetite is the dominant carrier of the ChRM. However, some samples had to be heated to 690 °C to determine a stable ChRM component, suggesting the presence of haematite. More than four successive points in the orthogonal diagrams (the ChRM directions with Maximum Angular Deviation [MAD] of <15°) were used to calculate the direction of the ChRM during the establishment of the polarity sequence (Figure 3). To remove outliers and transitional directions, we also rejected normal and reverse ChRM directions with Virtual Geomagnetic Poles (VGP) exceeding 45° from the mean normal and reverse VGP. Among the 1,729 discrete samples, 1,642 (95%) provided reliable ChRM directions and two magnetic components were isolated. The ChRM vector directions were used to define the polarity. The results indicate that the section records 19 normal (N1–N19) and 20 reversed (R1–R20) magnetozones (Figure 4a). This composite magnetic polarity sequence was correlated to the Geomagnetic Polarity Time Scale (Gradstein, Ogg, Schmitz, & Ogg, 2012) which suggests that the section has recorded a continuous geomagnetic polarity sequence from C5r.3r to C3r. The magnetostratigraphy provides reliable age control and can be used to estimate the average sediment accumulation rate between magnetic reversal boundaries (Figure 4b). Using this approach, we estimate that the section spans the interval from 11.8 to 5.8 Ma. A bed located at the depth of 128 m in the section contains a mammalian fossil assemblage that includes *Hipparion platyodus*, *Chilotherium* sp., *Gazella gaodryi*, *Palaeotragus* sp., and *Sinocastor*. These mammals all belong to the Baode stage in the Late Miocene (Gu et al., 1992) and provide an additional constraint on the age of the sequence and which is consistent with the palaeomagnetic dating.

The relationship between the stratigraphic depth and the magnetostratigraphic ages (Figure 4b) is almost linear which supports the validity of the magnetostratigraphy.

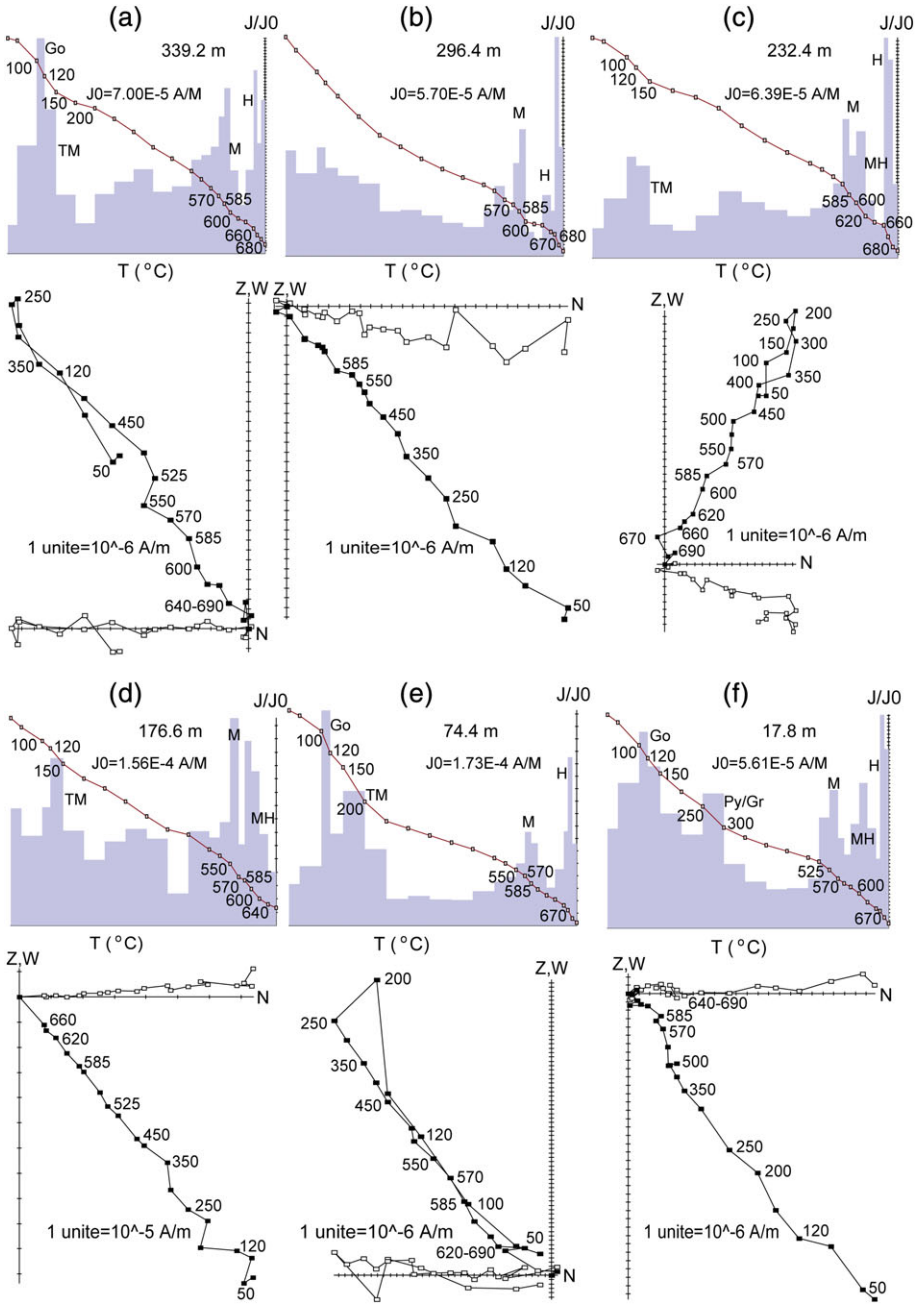

FIGURE 3 Representative thermal demagnetization diagrams for samples from the Jiarang section (directions are the original data in geographic coordinates). Temperature steps used are 25 °C, 50 °C, 100 °C, 120 °C, 150 C, 200 C, 250 °C, 300 °C, 350 °C, 400 °C, 450 °C, 500 °C, 525 °C, 550 °C, 570 °C, 585 °C, 600 °C, 620 °C, 640 °C, 660 °C, 670 °C, 680 °C, and 690 °C. Open (solid) symbols represent horizontal (vertical) projections; intensities are given in mA/m. J_0 = natural remanent magnetization; G = goethite; TM = titanomagnetite; MH = maghemite; M = magnetite; H = haematite

4.2 | Environmental proxies

4.2.1 | Magnetic susceptibility

Magnetic susceptibility in eolian sediments has been used as a proxy for the East Asian monsoon, with variations in MS interpreted as a measure of the summer monsoon intensity (An et al., 1990; An, Kukla, Porter, & Xiao, 1991). An intensified summer monsoon circulation promotes increased weathering and pedogenesis (An et al., 1991; Liu et al., 2004; Maher & Thompson, 1992; Sun et al., 2006; Zhou, Oldfield, Wintle, Robinson, & Wang, 1990). During pedogenesis, fine-grained magnetic minerals (dominantly single domain and superparamagnetic maghemite) are formed and enhance the MS. Although the exact origin of MS enhancement in eolian sediments is still debated, there is a consensus that the MS is a semi-quantitative or quantitative indicator of the amount of palaeorainfall, which is directly related to the EASM intensity (An et al., 1990; An et al., 2001; Ao et al., 2016; Bloemendal & Liu, 2005; Bloemendal, Liu, & Rolph, 1995; Hao & Guo, 2005; Kukla et al., 1988; Liu et al., 2004; Liu, Rolph, Bloemendal, Shaw, & Liu, 1995).

The MS record of the Jiarang Village section (Figure 5) can be divided into three intervals based on the pattern of fluctuations: (i) 361–152.2 m (11.8–8.5 Ma). The MS (χ_{lf}) values are relatively low (average of 17.728 × $10^{-8}$$m^3$ kg^{-1}), and there are high frequency

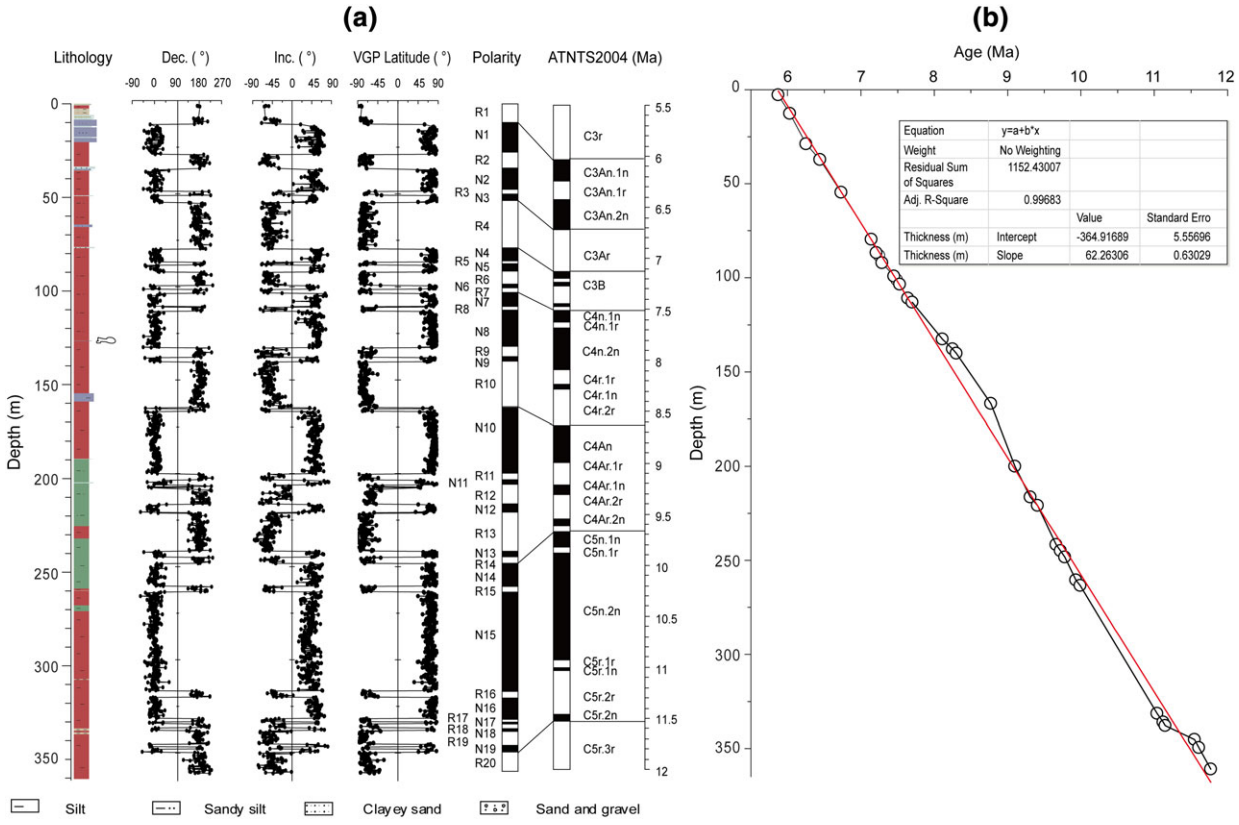

FIGURE 4 (a) Lithology and magnetostratigraphic results for the Jiarang section and correlation of the inferred polarity sequence with the Astronomically Tuned Neogene Time Scale (ATNT2004). (b) Age versus depth relationship for the Jiarang section based on the geomagnetic polarity stratigraphy

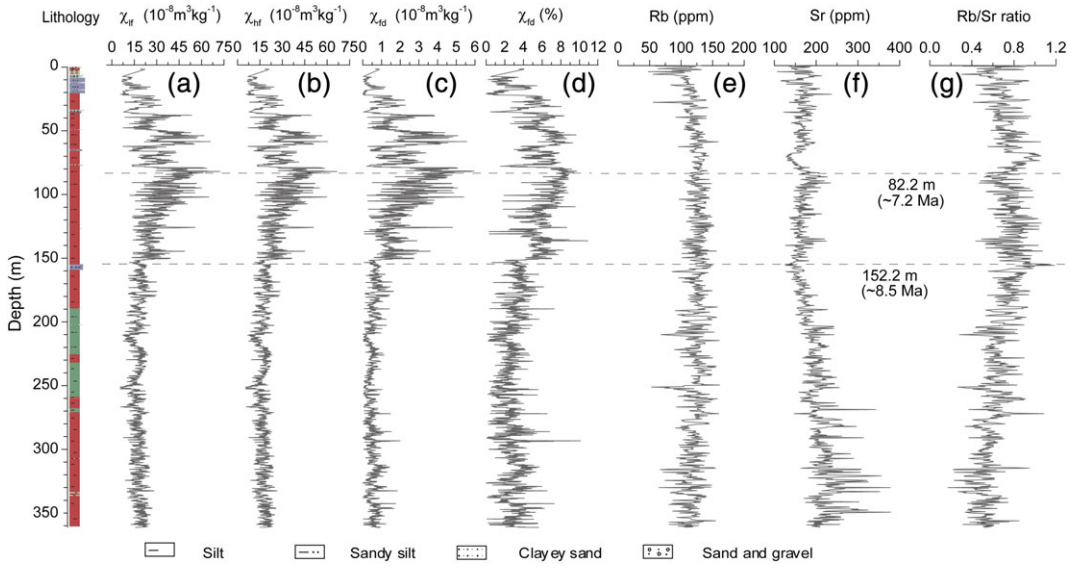

FIGURE 5 Times series of MS, Rb, and Sr concentrations and Rb/Sr ratio for the Jiarang section in the Jianzha Basin, north-eastern Tibetan Plateau. (a) Low frequency magnetic susceptibility (χ_{lf}). (b) High frequency magnetic susceptibility (χ_{hf}). (c) Mass specific frequency-dependent magnetic susceptibility (χ_{fd}). (d) Percentage frequency-dependent magnetic susceptibility (χ_{fd}%). (e) Rb concentration. (f) Sr concentration. (g) Rb/Sr ratio

fluctuations. (ii) 152.2–82.2 m (~8.5–7.2 Ma). The MS (χ_{lf}) values gradually increase to a maximum of 63.49 × $10^{-8}m^3$ kg^{-1} at the top of the interval and there are high frequency oscillations superimposed. (iii) 82.2–22.8 m (~7.2–6.2 Ma). The values gradually decrease with a pattern of lower frequency fluctuations superimposed. And it is can be seen that the MS (χ_{hf}, χ_{fd}, χ_{fd}%) shows mainly same variation trendency in the Figure 5. In general, χ_{fd} and χ_{fd}% show a similar pattern of variability to χ_{lf}. This is confirmed in Figure 6, which shows

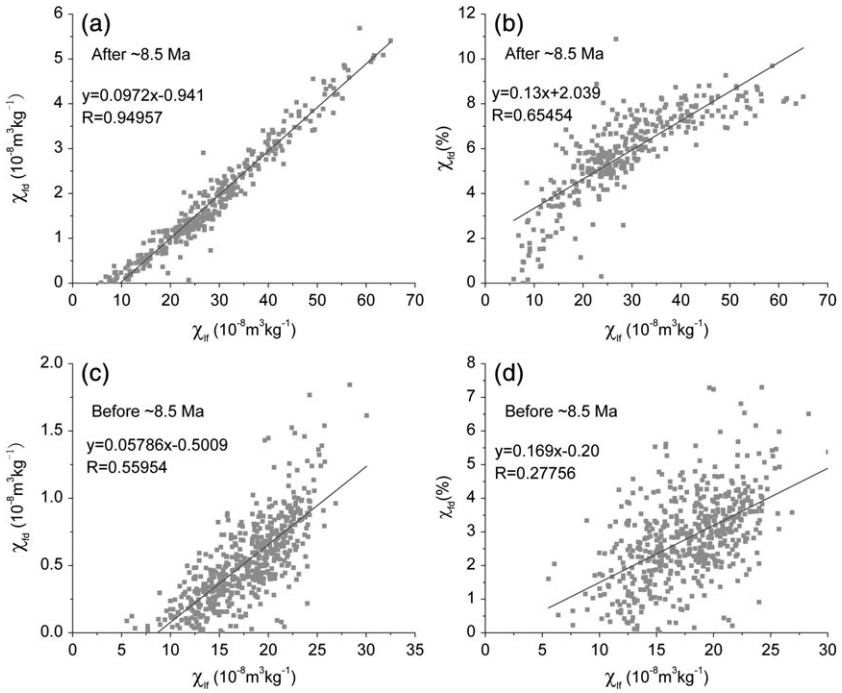

FIGURE 6 Scatterplots of χ_{lf} versus χ_{fd} and χ_{fd}%, after ~8.5 Ma (a,b) and before (c,d) ~8.5 Ma

scatterplots of the relationship between χ_{lf} and χ_{fd} and between χ_{lf} and χ_{fd}%. However, above the depth of 152.2 m (~8.5 Ma; Figure 6a,b), the relationship is significantly stronger (R = 0.957 for χ_{fd} and R = 0.655 for $\chi_{fd\%}$) than for the sediments older than ~8.5 Ma (R = 0.56 for χ_{fd} and R = 0.278 for χ_{fd}%). This indicates that the degree of weathering and pedogenesis was significantly stronger after ~8.5 Ma.

4.2.2 | Rb, Sr, and Rb/Sr ratio

Rubidium (Rb) and strontium (Sr) exhibit significantly different geochemical behaviour during chemical weathering, with Rb being more resistant. Therefore, variations in the Rb/Sr ratios in both loess and lacustrine sediments have been used as an index of chemical weathering intensity and hence of past climate (Chang et al., 2013; Chen, An, & Head, 1999; Du et al., 2011; Jin et al., 2001). In the context of the Jianzha Basin, the Rb/Sr ratio can be interpreted as reflecting variations in chemical weathering intensity in the basin, which are driven by variations in summer monsoon circulation.

The Rb and Sr concentrations and the Rb/Sr ratios vary significantly within the section. The Rb concentration ranges from 47.9 to 160.9 ppm and that for Sr ranges from 107 to 451.1 ppm, with averages of 121.36 and 187.9 ppm, respectively. The average content of Rb in the Jianzha section is similar to that in Upper Continental Crust (UCC; 110 ppm; Wedepohl, 1995), indicating that the sediments are well-mixed. However, the average content of Sr is lower than in UCC (316 ppm; Wedepohl, 1995), which indicates the loss of Sr in the Jianzha Basin. The Rb concentration is relatively stable throughout the section. However, the Sr concentration gradually decreases from ~11.8 to 8.57 Ma (with high amplitude fluctuations superimposed), is relatively stable from ~8.57 to 7.2 Ma, decreases rapidly within a relatively brief interval after ~7.2 Ma, and then recovers and maintains relatively stable values thereafter. The Rb/Sr ratio exhibits an inverse trend of variation to Sr from ~11.8 to 5.8 Ma, increasing from ~0.4 to ~1.2; thereafter, it exhibits a pattern of both high and low fluctuation variations within an overall range of ~0.4–0.9.

5 | DISCUSSION

The climates of Asia are significantly affected by the extent and height of the Himalayan Mountains and the TP (An et al., 2001; Kutzbach, Prell, & Ruddiman, 1993; Molnar et al., 1993). Recent $\delta^{18}O$ analyses of sedimentary carbonates reveal that since the Eocene the south Asian monsoonal moisture has not been able to reach the central TP owing to the southern topographic barrier (Caves et al., 2015); consequently, the precipitation and chemical weathering in the eastern TP were mainly controlled by the EASM in the Miocene. The EASM precipitation pattern in China is determined mainly by the jet stream's interaction with the TP (a mechanical effect) and by heating of the plateau (a thermal effect; An et al., 2015; Molnar, Boos, & Battisti, 2010; Wu et al., 2012). The TP interacts with the jet stream to steer the subtropical frontal system east of the TP, promoting precipitation in China (Molnar et al., 2010). The intensified heating associated with a high plateau can amplify the low-pressure system on the TP, amplifying the land–sea pressure contrast and causing additional precipitation in China (An et al., 2015; Wu et al., 2012). When the northern TP is low, these effects are weakened, resulting in decreased EASM precipitation (An et al., 2015; Liu, Kutzbach, Liu, An, & Li, 2003). Therefore, the upward and/or outward growth of the marginal portions of the TP will enable the EASM precipitation to penetrate further inland, as was recently demonstrated in model simulations (Zhang, Jiang, & Zhang, 2016). Sedimentological and thermochronological evidence reveals that the NETP experienced a phase of upward and/or outward growth during the Late Miocene (Molnar & Stock, 2009; Yuan et al., 2013). In the Miocene, the TP experienced a series of expansions to the north and to the east, and the mountain–basin system in the NETP

became surrounded by intermontane basins and mountains, including the eastern Kunlun–western Qinling Mountain, Altyn Tagh–South Qilian Mountain, and Liupan Mountain (Fang et al., 2005; Hough et al., 2014; Lease et al., 2011; Lease, Burbank, Hough, Wang, & Yuan, 2012; Molnar, 2005; Tapponnier et al., 2001). The published low-temperature thermochronological data reveal that a rapid exhumation occurred in the Liupan Shan and the north Qilian Shan areas, and sediment accumulation rate and provenance data in the Guide Basin reveal rapid exhumation of the Laji Shan during the Late Miocene (Fang et al., 2005; Zheng et al., 2006; Zheng, Clark, Zhang, Zheng, & Farley, 2010).

Time series of sediment accumulation rate (SAR), magnetic susceptibility (χ_{lf}), and Rb/Sr ratio for the Jiarang Village section are illustrated in Figure 7. Also shown for comparison is the marine oxygen isotope record ($\delta^{18}O$; Figure 7a; Zachos, Pagani, Sloan, Thomas, & Billups, 2001). The SAR record (Figure 7d) exhibits two intervals of rapid fluctuation between ~10 and ~6 Ma, which we interpret as a response to the series of uplifts and expansions to the north and to the east in the NETP in the Late Miocene. The EASM should have been strengthened by these events, and the increasing fluctuations in Rb/Sr ratio and MS before ~8.57 Ma may reflect intensified EASM precipitation which was impelled by the growth of the NETP (Figure 7b; An et al., 2001; Harrison, Copeland, Kidd, & Yin, 1992; Molnar et al., 1993). After ~8.57 Ma, and up to ~7.2 Ma, the periodic weakening of the EASM, as indicated by the Rb/Sr ratio, may indicate that the height of the TP was sufficient to obstruct the northward movement of the EASM, resulting in less precipitation in summer. However, the pronounced fluctuations in χ_{lf} during the interval from ~8.57 to ~7.2 Ma may indicate that weathering and pedogenesis were not the dominant factor driving the record, which may instead have been influenced by the increased input of lithogenic ferrimagnetic material. In addition, from ~7.2 Ma, the variation of the EASM record of the Jianzha Basin resembles the main trends in global temperature and ice accumulation reflected by the deep-sea oxygen isotope record (Figure 7a; Zachos et al., 2001). This indicates that the EASM was mainly controlled by global temperature changes from ~7.2 Ma onwards.

It is noteworthy that there is a lack of coherency between the fluctuations in χ_{lf} and Rb/Sr ratio between ~8.57 and ~7.21 Ma. In contrast, however, the Rb/Sr ratio and deep-sea oxygen isotope record fluctuate almost synchronously during the same interval. This indicates that there may have been a change in the provenance of the eolian Red Clay sediments in the Jianzha Basin at ~8.57 Ma which affected the magnetic properties. Fang (2007) considered that eolian dusts were gradually transported into the Linxia Basin after ~8.6 Ma, which also confirms that fresh clastic material was generated by weathering process in the northern TP (Yan, Miao, Zan, Zhang, & Wu, 2014). Recent studies reveal that the eolian sediments of the CLP are not necessarily derived from deserts and that deformation and uplift can produce dust for subsequent eolian transportation (Nie et al., 2014; Nie et al., 2015; Pullen et al., 2011). Thus, it is feasible that the Jianzha Basin began to receive eolian supply from material from the deformed and uplifted areas of the NETP at ~8.57 Ma.

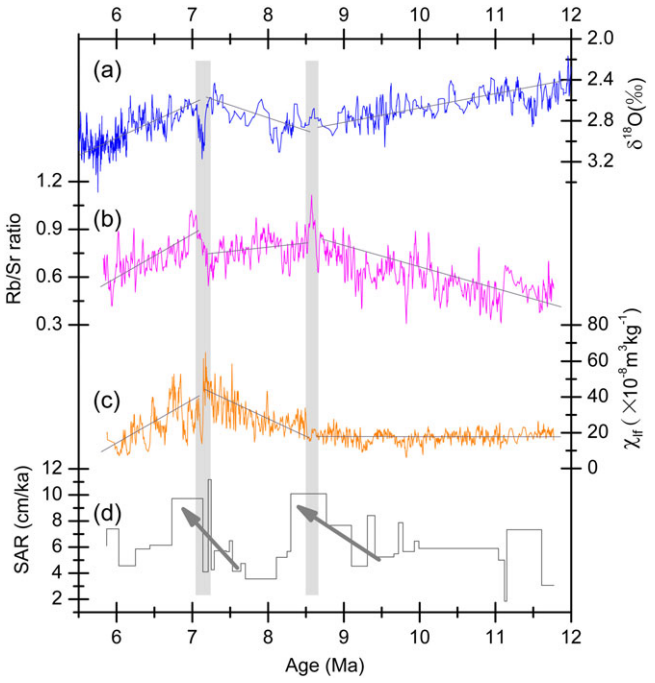

FIGURE 7 Comparison of palaeoenvironmental records from the Jiarang section in Jianzha Basin, north-eastern Tibetan Plateau, with the marine oxygen isotope record. (a) Global marine oxygen isotope record (Zachos et al., 2001). (b) Rb/Sr ratio for the Jiarang section (this study). (c) Magnetic susceptibility of the Jiarang section (this study). (d) Sediment accumulation rate for the Jiarang section (this study). The grey bars indicate major inflections in the records, and the arrows indicate two uplift stages around the Jianzha Basin

6 | CONCLUSIONS

1. Magnetostratigraphic results show that the Late Cenozoic sedimentary sequence from Jianzha Basin in the NETP has recorded a continuous geomagnetic polarity sequence from C5r.3r to C3r. Thus, the section spans the interval from 11.8 to 5.8 Ma in the Late Miocene.
2. There was an intensification of the EASM from at least 11.8 to ~8.57 Ma, and during this interval, the EASM was mainly controlled by the growth of the NETP. After ~8.57 Ma, and especially after ~7.2 Ma, the EASM was affected by global cooling and ice accumulation in the Northern Hemisphere.
3. Beginning of ~8.57 Ma, the eolian sediments in the Jianzha Basin were significantly affected by the supply of eolian material produced as a result of the deforming and uplifting areas of the TP.

ACKNOWLEDGMENTS

We thank Dr. Jan Bloemendal for discussions in detail and his revising manuscript, Mr. Mike O'Connor and Dong Junchao for their help with laboratory and field work, and Prof. Chang Hong for useful discussions. This study was supported by projects funded by the National Natural Science Foundation of China (Grants 40599420, 40872114, 41140028, 41572164, and 41772167); the Central University Research Foundation, Chang'an University (Grant 310827152014); and the State Key Laboratory of Loess and Quaternary Geology (Grant SKLLQG1601).

ORCID

Chaofeng Fu http://orcid.org/0000-0002-5056-4256

REFERENCES

An, Z. S. (2000). The history and variability of the East Asian paleomonsoon climate. *Quaternary Science Reviews*, *19*(1–5), 171–187.

An, Z. S., Colman, S. M., Zhou, W. J., Li, X. Q., Brown, E. T., Jull, A. J. T., … Xu, X. W. (2012). Interplay between the Westerlies and Asian monsoon recorded in Lake Qinghai sediments since 32 ka. *Scientific Reports*, *2*, 619. https://doi.org/10.1038/srep00619

An, Z. S., Kukla, G. J., Porter, S. C., & Xiao, J. L. (1991). Magnetic susceptibility evidence of monsoon variation on the Loess Plateau of central China during the last 130,000 years. *Quaternary Research*, *36*(1), 29–36.

An, Z. S., Kutzbach, J. E., Prell, W. L., & Porter, S. C. (2001). Evolution of Asian monsoons and phased uplift of the Himalayan Tibetan plateau since Late Miocene times. *Nature*, *411*(6833), 62–66.

An, Z. S., Liu, T. S., Lu, Y. C., Porter, S. C., Kukla, G., Wu, X. H., & Hua, Y. M. (1990). The long-term paleomonsoon variation recorded by the loess-paleosol sequence in Central China. *Quaternary International*, *s*, *7–8*, 91–95.

An, Z. S., Wu, G. X., Li, J. P., Sun, Y. B., Liu, Y. M., Zhou, W. J., … Mao, J. Y. (2015). Global monsoon dynamics and climate change. *Annual Review of Earth and Planetary Sciences*, *43*, 29–77.

An, Z. S., Zhang, P. Z., Wang, E. Q., Wang, S. M., Qiang, X. K., Li, L., … Ai, L. (2006). Change of the monsoon-arid environment in China and growth of the Tibetan Plateau since the Miocene (in Chinese). *Quaternary Science*, *26*(5), 678–693.

Ao, H., Roberts, A. P., Dekkers, M. J., Liu, X., Rohling, E. J., Shi, Z., … Zhao, X. (2016). Late Miocene–Pliocene Asian monsoon intensification linked to Antarctic ice-sheet growth. *Earth and Planetary Science Letters*, *444*, 75–87.

Bloemendal, J., & Liu, X. M. (2005). Rock magnetism and geochemistry of two Plio-Pleistocene Chinese loess–palaeosol sequences—Implications for quantitative palaeoprecipitation reconstruction. *Palaeogeography, Palaeoclimatology, Palaeoecology*, *226*(2), 149–166.

Bloemendal, J., Liu, X. M., & Rolph, T. C. (1995). Correlation of the magnetic susceptibility stratigraphy of Chinese loess and the marine oxygen isotope record: Chronological and palaeoclimatic implications. *Earth and Planetary Science Letters*, *131*(131), 371–380.

Caves, J. K., Winnick, M. J., Graham, S. A., Sjostrom, D. J., Mulch, A., & Chamberlain, C. P. (2015). Role of the westerlies in Central Asia climate over the Cenozoic. *Earth and Planetary Science Letters*, *428*, 33–43. https://doi.org/10.1016/j.epsl.2015.07.023

Chang, H., An, Z. S., Wu, F., Jin, Z. D., Liu, W. G., & Song, Y. G. (2013). A Rb/Sr record of the weathering response to environmental changes in westerly winds across the Tarim Basin in the late Miocene to the early Pleistocene. *Palaeogeography, Palaeoclimatology, Palaeoecology*, *386*(6), 364–373.

Chen, J., An, Z. S., & Head, J. (1999). Variation of Rb/Sr ratios in the loess-paleosol sequences of Central China during the last 130,000 years and their implications for monsoon paleoclimatology. *Quaternary Research*, *51*(3), 215–219.

Clift, P. D., Wan, S. M., & Blusztajn, J. (2014). Reconstructing chemical weathering, physical erosion and monsoon intensity since 25 Ma in the northern South China Sea: A review of competing proxies. *Earth-Science Reviews*, *130*, 86–102. https://doi.org/10.1016/j.earscirev.2014.01.002

Ding, Z. L., Rutter, N. W., Sun, J. M., Yang, S. L., & Liu, T. S. (2000). Re-arrangement of atmospheric circulation at about 2.6 Ma over Northern China: Evidence from grain size records of loess-palaeosol and red clay sequences. *Quaternary Science Reviews*, *19*(19), 547–558.

Ding, Z. L., Sun, J. M., Liu, T. S., Zhu, R. X., Yang, S. L., & Guo, B. (1998). Wind-blown origin of the Pliocene red clay formation in the central Loess Plateau, China. *Earth and Planetary Science Letters*, *161*(1–4), 135–143.

Du, S. H., Li, B. S., Niu, D. F., Zhang, D. D., Wen, X. H., Chen, D. N., … Wang, F. N. (2011). Age of the MGS5 segment of the Milanggouwan stratigraphical section and evolution of the desert environment on a kiloyear scale during the last interglacial in China's Salawusu River Valley: Evidence from Rb and Sr contents and ratios. *Chemie der Erde - Geochemistry*, *71*(1), 87–95.

Fang, X. M. (2007). High resolution rock magnetic records of Cenozoic sediments in the Linxia Basin and their implications on drying of Asian inland (in Chinese). *Quaternary Sciences*, *27*(6), 989–1000.

Fang, X. M., Yan, M. D., Van der Voo, R., Rea, D. K., Song, C. H., Parés, J. M., … Dai, S. (2005). Late Cenozoic deformation and uplift of the NE Tibetan Plateau: Evidence from high-resolution magnetostratigraphy of the Guide Basin, Qinghai Province, China. *Geological Society of America Bulletin*, *117*(9–10), 1208–1225.

Fu, C. F., An, Z. S., Qiang, X. K., Bloemendal, J., Song, Y. G., & Chang, H. (2013). Magnetostratigraphic determination of the age of ancient Lake Qinghai, and record of the East Asian monsoon since 4.63 Ma. *Geology*, *41*(8), 875–878. https://doi.org/10.1130/g34418.1

Fu, C. F., Bloemendal, J., Qiang, X. K., Hill, M. J., & An, Z. S. (2015). Occurrence of greigite in the Pliocene sediments of Lake Qinghai, China, and its paleoenvironmental and paleomagnetic implications. *Geochemistry, Geophysics, Geosystems*, *16*(5), 1293–1306.

Gradstein, F., Ogg, J. G., Schmitz, M., & Ogg, G. (2012). The geologic time scale 2012 2-volume set: Elsevier.

Gu, Z. G., Bai, S. H., Zhang, X. T., Ma, Y. Z., Wang, S. H., & Li, B. Y. (1992). Neogene subdivision and correlation of sediments within the Guide and Hualong basins of Qinghai province (in Chinese). *Journal of Stratigraphy*, *16*(2), 96–104.

Guo, Z. T., Liu, T. S., Fedoroff, N., Wei, L. Y., Ding, Z. L., Wu, N. Q., … An, Z. S. (1998). Climate extremes in loess of China coupled with the strength of deep-water formation in the North Atlantic. *Global and Planetary Change*, *18*(3–4), 113–128.

Guo, Z. T., Ruddiman, W. F., Hao, Q. Z., Wu, H. B., Qiao, Y. S., Zhu, R. X., … Liu, T. S. (2002). Onset of Asian desertification by 22 Myr ago inferred from loess deposits in China. *Nature*, *416*(6877), 159–163.

Hao, Q. Z., & Guo, Z. T. (2005). Spatial variations of magnetic susceptibility of Chinese loess for the last 600 kyr: Implications for monsoon evolution. *Journal of Geophysical Research Atmospheres*, *110*(B12), 501–509.

Harrison, T. M., Copeland, P., Kidd, W. S., & Yin, A. (1992). Raising Tibet. *Science*, *255*(5052), 1663–1670.

Hough, B. G., Garzione, C. N., Wang, Z., & Lease, R. O. (2014). Timing and spatial patterns of basin segmentation and climate change in northeastern Tibet. *Geological Society of America Special Papers*, *507*, SPE507–SPE507.

Jin, Z. D., Wang, S. M., Shen, J., Zhang, E. L., Li, F. C., Ji, J. F., & Lu, X. W. (2001). Chemical weathering since the Little Ice Age recorded in lake sediments: A high-resolution proxy of past climate. *Earth Surface Processes and Landforms*, *26*(7), 775–782.

Kirschvink, J. (1980). The least-squares line and plane and the analysis of palaeomagnetic data. *Geophysical Journal of the Royal Astronomical Society*, *62*(3), 699–718.

Kukla, G., Heller, F., Liu, X. M., Xu, T. C., Liu, T. S., & An, Z. S. (1988). Pleistocene climates in China dated by magnetic susceptibility. *Geology*, *16*(9), 811–814.

Kutzbach, J. E., Guetter, P. J., Ruddiman, W. F., & Prell, W. L. (1989). Sensitivity of climate to late Cenozoic uplift in southern Asian and the American west: Numerical experiments. *Journal of Geophysical Research-Atmospheres*, *94*(D15), 18393–18407. https://doi.org/10.1029/JD094iD15p18393

Kutzbach, J. E., Prell, W. L., & Ruddiman, W. F. (1993). Sensitivity of Eurasian climate to surface uplift of the Tibetan Plateau. *The Journal of Geology*, *101*(2), 177–190.

Lease, R. O., Burbank, D. W., Clark, M. K., Farley, K. A., Zheng, D., & Zhang, H. (2011). Middle Miocene reorganization of deformation along the northeastern Tibetan Plateau. *Geology*, *39*(4), 359–362.

Lease, R. O., Burbank, D. W., Hough, B., Wang, Z. C., & Yuan, D. Y. (2012). Pulsed Miocene range growth in northeastern Tibet: Insights from Xunhua Basin magnetostratigraphy and provenance. *Geological Society of America Bulletin*, *124*(5–6), 657–677. https://doi.org/10.1130/b30524.1

Li, J. J. (1991). The environmental effects of the uplift of the Qinghai-Xizang Plateau. *Quaternary Science Reviews*, *10*(6), 479–483.

Li, J. J., & Fang, X. M. (1999). Uplift of the Tibetan Plateau and environmental changes. *Chinese Science Bulletin*, *44*(23), 2117–2124.

Li, J. J., Feng, Z. D., & Tang, L. Y. (1988). Late Quaternary monsoon patterns on the Loess Plateau of China. *Earth Surface Processes and Landforms*, *13*(2), 125–135.

Liu, Q. S., Jackson, M. J., Banerjee, S. K., Maher, B. A., Deng, C. L., Pan, Y. X., & Zhu, R. X. (2004). Mechanism of the magnetic susceptibility enhancements of the Chinese loess. *Journal of Geophysical Research - Solid Earth*, *109*(B12), B12107–B12116.

Liu, X. D., Guo, Q. C., Guo, Z. T., Yin, Z. Y., Dong, B. W., & Smith, R. B. (2015). Where were the monsoon regions and arid zones in Asia prior to the Tibetan Plateau uplift? [Review]. *National Science Review*, *2*(4), 403–416. https://doi.org/10.1093/nsr/nwv068

Liu, X. D., Kutzbach, J. E., Liu, Z. Y., An, Z. S., & Li, L. (2003). The Tibetan Plateau as amplifier of orbital-scale variability of the East Asian monsoon. *Geophysical Research Letters*, *30*(16), 337–356.

Liu, X. M., Rolph, T., Bloemendal, J., Shaw, J., & Liu, T. S. (1995). Quantitative estimates of palaeoprecipitation at Xifeng, in the Loess Plateau of China. *Palaeogeography, Palaeoclimatology, Palaeoecology*, *113*(2), 243–248.

Liu, X. M., Shaw, J., Jiang, J. Z., Bloemendal, J., Hesse, P., Rolph, T., & Mao, X. G. (2010). Analysis on variety and characteristics of maghemite. *Science China Earth Sciences*, *53*(8), 1153–1162.

Lu, H. Y., & Guo, Z. T. (2014). Evolution of the monsoon and dry climate in East Asia during late Cenozoic: A review. *Science China Earth Sciences*, *57*(1), 70–79. https://doi.org/10.1007/s11430-013-4790-3

Maher, B. A., & Thompson, R. (1992). Paleoclimatic significance of the mineral magnetic record of the Chinese loess and paleosols. *Geology*, *37*(2), 155–170.

Métivier, F., Gaudemer, Y., Tapponnier, P., & Meyer, B. (1998). Northeastward growth of the Tibet plateau deduced from balanced reconstruction of two depositional areas: The Qaidam and Hexi Corridor basins, China. *Tectonics*, *17*(6), 823–842.

Molnar, P. (2005). The growth of the Tibetan Plateau and Mio-Pliocene evolution of East Asian climate. *Palaeontologia Electronica*, *8*(1), 131–142.

Molnar, P., Boos, W. R., & Battisti, D. S. (2010). Orographic controls on climate and paleoclimate of Asia: Thermal and mechanical roles for the Tibetan Plateau. *Annual Review of Earth and Planetary Sciences*, *38*(1), 77–102.

Molnar, P., England, P., & Martinod, J. (1993). Mantle dynamics, uplift of the Tibetan Plateau, and the Indian monsoon. *Reviews of Geophysics*, *31*(4), 357–396.

Molnar, P., & Lyon-Caent, H. (1989). Fault plane solutions of earthquakes and active tectonics of the Tibetan Plateau and its margins. *Geophysical Journal International*, *99*(1), 123–154.

Molnar, P., & Stock, J. M. (2009). Slowing of India's convergence with Eurasia since 20 Ma and its implications for Tibetan mantle dynamics. *Tectonics*, *28*. TC3001. https://doi.org/10.1029/2008TC002271

Nie, J. S., Garzione, C., Su, Q. D., Liu, Q. S., Zhang, R., Heslop, D., … Luo, Z. (2017). Dominant 100,000-year precipitation cyclicity in a late Miocene lake from northeast Tibet. *Science Advances*, *3*(3). e1600762. https://doi.org/10.1126/sciadv.1600762

Nie, J. S., Peng, W. B., Möller, A., Song, Y. G., Stockli, D. F., Stevens, T., … Oalmann, J. (2014). Provenance of the upper Miocene–Pliocene Red Clay deposits of the Chinese loess plateau. *Earth and Planetary Science Letters*, *407*(407), 35–47.

Nie, J. S., Stevens, T., Rittner, M., Stockli, D., Garzanti, E., Limonta, M., … Saylor, J. (2015). Loess plateau storage of northeastern Tibetan plateau-derived Yellow River sediment. *Nature Communications*, *6*(1), 8511. https://doi.org/10.1038/ncomms9511

Prell, W. L., & Kutzbach, J. E. (1992). Sensitivity of the Indian monsoon to forcing parameters and implications for its evolution. *Nature*, *360*(6405), 647–652.

Pullen, A., Kapp, P., Mccallister, A. T., Chang, H., Gehrels, G. E., Garzione, C. N., … Ding, L. (2011). Qaidam Basin and northern Tibetan Plateau as dust sources for the Chinese Loess Plateau and paleoclimatic implications. *Geology*, *39*(11), 1031–1034.

Qiang, X. K., An, Z. S., Song, Y. G., Chang, H., Sun, Y. B., Liu, W. G., … Ai, L. (2011). New eolian red clay sequence on the western Chinese Loess Plateau linked to onset of Asian desertification about 25 Ma ago. *Science in China Series D: Earth Sciences*, *54*(1), 136–144.

Qiang, X. K., Li, Z. X., Powell, C. M., & Zheng, H. B. (2001). Magnetostratigraphic record of the Late Miocene onset of the East Asian monsoon, and Pliocene uplift of northern Tibet. *Earth and Planetary Science Letters*, *187*(1–2), 83–93.

Raymo, M., & Ruddiman, W. F. (1992). Tectonic forcing of late Cenozoic climate. *Nature*, *359*(6391), 117–122.

Rea, D. K., Snoeckx, H., & Joseph, L. H. (1998). Late Cenozoic eolian deposition in the North Pacific: Asian drying, Tibetan uplift, and cooling of the northern hemisphere. *Paleoceanography*, *13*(3), 215–224.

Shi, Y. F., Tang, M. C., & Ma, Y. Z. (1999). Linkage between the second uplifting of the Qinghai-Xizang (Tibetan) Plateau and the initiation of the Asian monsoon system. *Science in China Series D: Earth Sciences*, *42*(3), 303–312.

Song, C. H., Fang, X. M., Gao, J. P., Sun, D., & Fan, M. J. (2001). Tectonic uplift and sedimentary evolution of the Guide Basin in the northeast margin of Tibetan Plateau in Cenozoic Era. *Acta Sedimentologica Sinica*, *19*(4), 493–500. https://doi.org/10.14027/J.cnki.cjxb.2001.04.003

Song, C. H., Hu, S. H., Han, W. X., Zhang, T., Fang, X. M., Gao, J. P., & Wu, F. L. (2014). Middle Miocene to earliest Pliocene sedimentological and geochemical records of climate change in the western Qaidam Basin on the NE Tibetan Plateau. [Article]. *Palaeogeography, Palaeoclimatology, Palaeoecology*, *395*, 67–76. https://doi.org/10.1016/j.palaeo.2013.12.022

Sun, D. H., Shaw, J., An, Z. S., Cheng, M. Y., & Yue, L. P. (1998). Magnetostratigraphy and paleoclimatic interpretation of a continuous 7.2 Ma Late Cenozoic eolian sediments from the Chinese Loess Plateau. *Geophysical Research Letters*, *25*(1), 85–88.

Sun, J. Z. (2005). *Loessology* (Vol. I). Hongkong: The Hong Kong archaeology society.

Sun, X. J., & Wang, P. X. (2005). How old is the Asian monsoon system? Palaeobotanical records from China. [Review]. *Palaeogeography, Palaeoclimatology, Palaeoecology*, *222*(3–4), 181–222. https://doi.org/10.1016/j.palaeo.2005.03.005

Sun, Y. B., An, Z. S., Clemens, S. C., Bloemendal, J., & Vandenberghe, J. (2010). Seven million years of wind and precipitation variability on the Chinese Loess Plateau. *Earth and Planetary Science Letters*, *297*(3–4), 525–535.

Sun, Y. B., Chen, J., Clemens, S. C., Liu, Q. S., Ji, J. f., & Tada, R. J. (2006). East Asian monsoon variability over the last seven glacial cycles recorded by a loess sequence from the northwestern Chinese Loess Plateau. *Geochemistry, Geophysics, Geosystems*, *7*(12), 97–112.

Sun, Y. B., Ma, L., Bloemendal, J., Clemens, S., Qiang, X. K., & An, Z. S. (2015). Miocene climate change on the Chinese Loess Plateau: Possible links to the growth of the northern Tibetan Plateau and global cooling. *Geochemistry, Geophysics, Geosystems*, *16*(7), 2097–2108. https://doi.org/10.1002/2015gc005750

Tapponnier, P., Meyer, B., Avouac, J. P., Peltzer, G., Gaudemer, Y., Guo, S., … dai, H. G. (1990). Active thrusting and folding in the Qilian Shan, and decoupling between upper crust and mantle in northeastern Tibet. *Earth and Planetary Science Letters*, *97*(3–4), 382–383. 387-403

Tapponnier, P., Xu, Z. Q., Roger, F., Meyer, B., Arnaud, N., Wittlinger, G., & Yang, J. S. (2001). Oblique stepwise rise and growth of the Tibet Plateau. *Science*, *294*(5547), 1671–1677.

Thompson, R., & Oldfield, F. (1986). *Environmental magnetism*. London: Allen & Unwin.

Wan, S. M., Clift, P. D., Li, A. C., Li, T. G., & Yin, X. B. (2010). Geochemical records in the South China Sea: Implications for East Asian summer monsoon evolution over the last 20 Ma. In P. D. Clift, R. Tada, & H. Zheng (Eds.), Monsoon evolution and tectonics: Climate linkage in Asia Vol. 342 (pp. 245–263). Bath: Geological Soc Publishing House.

Wedepohl, K. H. (1995). The composition of the continental crust. *Geochimica et Cosmochimica Acta*, *59*(7), 1217–1232.

Wu, G. X., Liu, Y. M., He, B., Bao, Q., Duan, A. M., & Jin, F. F. (2012). Thermal controls on the Asian summer monsoon. *Scientific Reports*, *2*(5), 404. https://doi.org/10.1038/srep00404

Yan, X. L., Miao, Y. F., Zan, J. B., Zhang, W. L., & Wu, S. (2014). Late Cenozoic fluvial-lacustrine susceptibility increases in the Linxia Basin and their implications for Tibetan Plateau uplift. *Quaternary International*, *334*, 132–140. https://doi.org/10.1016/j.quaint.2013.12.046

Yin, A. (2010). Cenozoic tectonic evolution of Asia: A preliminary synthesis. *Tectonophysics*, *488*(1–4), 293–325.

Yuan, D. Y., Ge, W. P., Chen, Z. W., Li, C. Y., Wang, Z. C., Zhang, H. P., … Craddock, W. H. (2013). The growth of northeastern Tibet and its relevance to large-scale continental geodynamics: A review of recent studies. *Tectonics*, *32*(5), 1358–1370.

Zachos, J., Pagani, M., Sloan, L., Thomas, E., & Billups, K. (2001). Trends, rhythms, and aberrations in global climate 65 Ma to present. *Science*, *292*(5517), 686–693. https://doi.org/10.1126/science.1059412

Zhang, R., Jiang, D. B., & Zhang, Z. S. (2016). The impact of the uplifts of the main part and marginal area of the Tibetan Plateau on the Asian monsoon climate. *Quaternary Sclence*, *36*(4), 945–952.

Zhang, Z. S., Wang, H. J., Guo, Z. T., & Jiang, D. B. (2007). What triggers the transition of palaeoenvironmental patterns in China, the Tibetan Plateau uplift or the Paratethys Sea retreat? *Palaeogeography, Palaeoclimatology, Palaeoecology*, *245*(4), 317–331.

Zheng, D. W., Clark, M. K., Zhang, P. Z., Zheng, W. J., & Farley, K. A. (2010). Erosion, fault initiation and topographic growth of the North Qilian Shan (northern Tibetan Plateau). *Geosphere*, *6*(6), 937–941.

Zheng, D. W., Zhang, P. Z., Wan, J. l., Yuan, D. Y., Li, C. Y., Yin, G. M., … Chen, J. (2006). Rapid exhumation at ~ 8Ma on the Liupan Shan thrust fault from apatite fission-track thermochronology: Implications for growth of the northeastern Tibetan Plateau margin. *Earth and Planetary Science Letters*, *248*(1–2), 198–208.

Zhou, L. P., Oldfield, F., Wintle, A. G., Robinson, S. G., & Wang, J. T. (1990). Partly pedogenic origin of magnetic variations in Chinese loess. *Nature*, *346*(6286), 737–739.

Zijderveld, J. (1967). AC demagnetization of rocks: Analysis of results. *Methods in paleomagnetism*, *3*, 254–286.

How to cite this article: Fu C, Qiang X, Xu X, Xi J, Zuo J, An Z. Late Miocene magnetostratigraphy of Jianzha Basin in the northeastern margin of the Tibetan Plateau and changes in the East Asian summer monsoon. *Geological Journal*. 2018;53(S1): 282–292. https://doi.org/10.1002/gj.3047